Adaptive energy shaping control of a class of nonlinear soft continuum manipulators

E. Franco*, A. Garriga-Casanovas, J. Tang, F. Rodriguez y Baena, A. Astolfi, *Fellow, IEEE*

***Abstract*—Soft continuum manipulators are characterized by low stiffness which allows safe operation in unstructured environments but introduces under-actuation. In addition, soft materials such as silicone rubber, which are commonly used for soft manipulators, are characterized by nonlinear stiffness, while pneumatic actuation can result in nonlinear damping. Consequently, achieving accurate control of these systems in the presence of disturbances is a challenging task. This paper investigates the model-based adaptive control for soft continuum manipulators that have nonlinear uniform stiffness and nonlinear damping, that bend under the effect of internal pressure, and that are subject to time-varying disturbances. A rigid-link model with virtual elastic joints is employed for control purposes within the port-Hamiltonian framework. The effects of disturbances and of model uncertainties are estimated adaptively. A nonlinear controller that regulates the tip orientation of the manipulator and that compensates the effects of disturbances and of model uncertainties is then constructed by using an energy shaping passivity-based approach. Stability conditions are discussed highlighting the beneficial role of nonlinear damping. The effectiveness of the controller is assessed with simulations and with experiments on a soft continuum manipulator prototype.**

***Index Terms*—Robot Control, Soft Robotics, Adaptive Control, Nonlinear Control Systems.**

I. Introduction

Soft continuum manipulators are a class of systems characterized by high dexterity, light weight, and low stiffness. Thanks to these desirable features, they are ideally suited for minimally invasive surgery, collaborative manipulation, and navigation in cluttered environments [1]. Popular actuation strategies for soft continuum manipulators include pneumatics [2], hydraulics [3], and tendon driven mechanisms [4]. Alternative approaches include dielectric elastomers [5] and shape-memory alloys [6]. Pneumatics has been one of the most common strategies due to its fast response, high power density, affordable cost, and ease of miniaturization. Recently, pneumatics has also been employed to provide position and contact sensing in soft manipulators [7]. Regardless of the actuation principle, soft continuum manipulators are typically underactuated since they experience continuous deformation along their length, and since only a limited number of control actions are generally available. Additionally, only few degrees-of-freedom (DOFs) are directly measurable with sensors. Thus controlling soft continuum manipulators is a challenging problem that has attracted increasing attention in the research community [8].

Numerical model-free controllers represent a pragmatic solution and are particularly beneficial when knowledge of the system is limited [9], [10]. However, this approach can be computationally expensive and can rely heavily on training data, thus it might not be viable in some applications. Model-based controllers are often preferred when fast control and high accuracy are required [2]. The preferred modelling approaches for control purposes due to their computational efficiency include the constant-curvature (CC) model, the piecewise constant-curvature (PCC) model [11], and the rigid-link model [12]. CC and PCC are model-reduction techniques that allow treating the system as fully actuated, which is a suitable approach if external disturbances are negligible. Notable alternatives, including discrete Cosserat models [13]–[15] and order reduction of finite element models [16], [17], provide more accurate descriptions of the system in quasi-static conditions but are less suitable for fast control. Classical controllers for CC models of continuum manipulators include optimal control [18], sliding mode control, model predictive control [19], [20], and feedback linearization [2]. Preserving performance of classical controllers in the presence of disturbances typically requires high gains, which however can increase the stiffness of soft manipulators in closed loop, as observed in [21]. This undesirable effect has prompted the study of feed-forward control actions, first for planar PCC models [22], and more recently by employing a polynomial approximation of the curvature thus yielding a nonlinear controller [23]. Feed-forward control has also been employed for fully actuated continuous manipulators in [24] and to compensate the effects of nonlinearities in [25]. Accounting for nonlinear stiffness and nonlinear damping within the controller has proved beneficial in several settings, including

This research was supported by the Engineering and Physical Sciences Research Council (grant number EP/R009708/1 and EP/R511547/1). A. Astolfi is also supported by the European Union's Horizon 2020 Research and Innovation Programme under grant agreement No 739551 (KIOS CoE).

E. Franco (*corresponding author), A. Garriga Casanovas, and F. Rodriguez y Baena are with the Mechatronics in Medicine Laboratory, Mechanical Engineering Department, Imperial College London, Exhibition Road, SW7 2AZ, UK (e-mail: e.franco11@imperial.ac.uk, a.garriga-casanovas14@imperial.ac.uk, f.rodriguez@imperial.ac.uk).

J. Tang is with the Electrical and Electronic Engineering Department, Imperial College London, UK (e-mail: jacky.tang18@imperial.ac.uk).

A. Astolfi is with the Electrical and Electronic Engineering Department, Imperial College London, UK, and with the Dipartimento di Ingegneria Civile e Ingegneria Informatica, Università di Roma "Tor Vergata" Rome, 00133, Italy (e-mail: a.astolfi@imperial.ac.uk).

suspension systems [26]. While the former model-based controllers are effective within their respective assumptions, they are designed for fully actuated models and they do not include the adaptive compensation of unknown disturbances.

This paper investigates the energy shaping control of a class of underactuated mechanical systems with nonlinear uniform stiffness and nonlinear damping that are representative of soft continuum manipulators in 3D space. To this end the port-Hamiltonian formulation and the method of *Interconnection and Damping Assignment Passivity Based Control* (IDA-PBC) [27] are employed. The port-Hamiltonian formulation is widely applicable to a variety of systems, including soft robots [28]. The IDA-PBC method does not require high gains, but it relies on the exact knowledge of the system model and it aims to shape the energy of the closed-loop system with an appropriate control action in order to stabilize the prescribed equilibrium [27]. IDA-PBC has traditionally been applied to underactuated systems without physical damping and with a limited number of DOFs. An initial energy shaping controller for underactuated planar soft manipulators with linear stiffness and linear damping has been proposed in [29]. An extension to 3D space has been presented in [30], which however assumes constant disturbances. These results are extended here for soft continuum manipulators with nonlinear uniform stiffness and subject to time-varying disturbances affecting all DOFs. The main contributions of this work include the following points.

1. A partial-state feedback control law constructed with the IDA-PBC method for a generic $2n+1$ DOFs model with nonlinear uniform stiffness. The controller ensures local asymptotic stability of the desired equilibrium.
2. The definition of a class of underactuated mechanical systems representative of soft continuum manipulators for which the proposed controller is implementable.
3. An adaptive algorithm that combines the *Immersion and Invariance* (I&I) method [31], [32] and the *congelation of variables* approach [33] to compensate the effects of time-varying non-vanishing unknown disturbances.
4. The study of the stability conditions and their relationship with the tuning parameters. Although damping has traditionally been considered an obstacle in energy shaping control of underactuated systems [34], this study highlights its stabilizing effects for soft continuum manipulators.
5. Numerical simulations and experiments on a prototype with pneumatic actuation in different operating conditions.

A preliminary version of portions of this work appeared in conference form in [30], which discussed the regulation of the tip orientation in 3D for a simplified model with linear stiffness and linear damping considering the theoretical case of constant disturbances. This study significantly extends [30] by considering systems with nonlinear stiffness and nonlinear damping and by accounting for time-varying disturbances, thus resulting in a new nonlinear controller, in explicit stability conditions, and in corresponding tuning guidelines.

The rest of the paper is organized as follows. Section II presents the system model and the problem statement; Section III details the controller design and discusses the stability conditions; Section IV presents the simulation result and the experimental results; Section V contains concluding remarks.

II. Problem Formulation

A. Soft Continuum Manipulator

This work focusses on soft continuum manipulators with pneumatic actuation similar to that presented in [35]. The manipulator has a tubular structure made of a hyper-elastic material with a constant cross section, as shown in Figure 1. The cross section defines three equal internal chambers spaced at $120°$, similarly to the design in [36]. An inextensible nylon fiber is embedded at the center of the cross section along the device to prevent elongation of its neutral axis. A second inextensible fiber is wound around the device to prevent radial expansion of the outer wall while allowing bending. Full details of the design and manufacturing process appear in [35].

The base of the manipulator is fixed and, by controlling the pressures P_0, P_1 and P_2 in the internal chambers, the device can bend in any plane, while length and external diameter are assumed constant. At equilibrium and without disturbances, the orientation of the bending plane φ and the rotation of the tip θ on the bending plane are given as in [36]

$$\theta = \frac{1}{k^*\sqrt{2}}\sqrt{(P_1-P_2)^2+(P_1-P_0)^2+(P_2-P_0)^2}, \quad (1.a)$$

$$\tan(\varphi) = \frac{\sqrt{3}(P_1-P_2)}{P_1+P_2-2P_0}, \quad (1.b)$$

where k^* is the structural bending stiffness of the manipulator expressed in bar/rad, assumed uniform over the whole length. The resultant pressure vector computed from P_0, P_1, P_2 in a fixed reference frame (see Figure 1.b) is defined by magnitude and direction which correspond to two control inputs u_I, u_{II}. The relationships between P_0, P_1, P_2 and u_I, u_{II} are

$$u_I = \frac{1}{\sqrt{2}}\sqrt{(P_1-P_2)^2+(P_1-P_0)^2+(P_2-P_0)^2}, \quad (2.a)$$

$$u_{II} = \frac{\sqrt{3}(P_1-P_2)}{P_1+P_2-2P_0}. \quad (2.b)$$

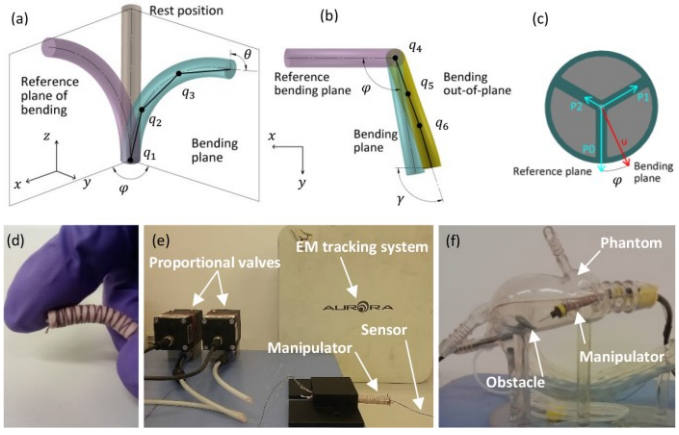

Figure 1. CAD model and rigid-link model of a continuum manipulator with $n = 3$ (a); model top view (b); cross section (c). Prototype (d); experimental test setup (e); additional test setup shown in the Supplementary Video (f).

B. System Model

For control purposes the soft continuum manipulator is modelled as a rigid-link underactuated system consisting of $2n+1$ virtual elastic pin joints (see Figure 1). The n links have equal length and equal mass concentrated at their midpoint. The total mass of the manipulator is m_T and the total length is L_T. This approximation has been used for other soft continuum manipulators [12] since it is more general than the CC model, which is not suitable in the presence of external disturbances [29]. The discrepancy between the model and the real system, and the effect of external forces on the virtual joints are accounted for in this work by the unknown lumped disturbance $\delta \in \mathbb{R}^{2n+1}$. Without loss of generality, the system dynamics is expressed in port-Hamiltonian form as

$$\begin{bmatrix}\dot{q}\\ \dot{p}\end{bmatrix} = \begin{bmatrix}0 & I\\ -I & -R\end{bmatrix}\begin{bmatrix}\nabla_q H\\ \nabla_p H\end{bmatrix} + \begin{bmatrix}0\\ G\end{bmatrix}u - \begin{bmatrix}0\\ \delta\end{bmatrix}, \tag{3}$$

where the Hamiltonian is $H = T(q,p) + V(q)$, with kinetic energy $T(q,p) = \frac{1}{2}p^T M^{-1} p$, and potential energy $V(q)$. The inertia matrix $M(q) = M^T(q) > 0$ is bounded and has elements that depend on q_i [12], [29]. The system states are the angular position $q(t) \in \mathbb{R}^{2n+1}$ of the virtual joints and the momenta $p = M\dot{q}$. The symbols $\nabla_q H$ and $\nabla_p H$ are the vectors of partial derivatives of H with respect to q and to p, and I is the identity matrix. The effect of the pressure dynamics is approximated by the damping matrix $R > 0$. This is motivated by the small volume of the internal chambers ($\ll 1$ ml) and by the fast response (≤ 10 ms) and large flow rate ($\gg 10$ l/s) of the pressure regulators in our test setup (see Section IV.B).

The port-Hamiltonian representation (3) highlights the effect of the control action u in terms of mechanical energy, which is exploited for the controller design in Section III.A. The joint angles q_1 to q_n are relative to the previous link on the bending plane and define the tip rotation $\theta = \sum_{i=1}^{n} q_i$. The corresponding out-of-plane angles q_{n+1} to q_{2n} define the rotation outside the bending plane $\omega = \sum_{i=n+1}^{2n} q_i$. The orientation of the bending plane relative to a fixed reference frame is $q_{2n+1} = \varphi$, while the tip rotation in the direction orthogonal to the bending plane is $\gamma = \sum_{i=n+1}^{2n+1} q_i$. Twist is assumed negligible since it is not actuated in the manipulator [35] and since this work considers external forces that do not generate twist. In general, twist can be actuated by employing a different manipulator design, such as that in [36], which shall be investigated in our future work. The control input $u(t) \in \mathbb{R}^2$ depends on the pressures according to (2), and the input matrix is $G^T = \begin{bmatrix}1_n & 0_n & 0\\ 0_n & 0_n & 1\end{bmatrix}$, with $\mathrm{rank}(G) = 2$, where $[1_n], [0_n]$ are row vectors of length n. The class of systems studied in this work is defined by the following assumptions.

Assumption 1: Only the tip angles θ and γ and their first order time derivatives are known at any instant. In addition $|\theta| \leq Q_I$ and $|\gamma| \leq Q_{II}$ for some $Q_I > 0$ and $Q_{II} > 0$. In our setup the angles θ and γ are measured with an electromagnetic tracking system and a sensor mounted at the tip of the manipulator, while $\dot{\theta}$ and $\dot{\gamma}$ are computed by differentiation. However, different sensors could be employed. Finally, for our prototype $Q_I = Q_{II} = \pi/2$ in the absence of external forces.

Assumption 2: The potential energy is defined as $V(q) = \sum_{i=1}^{n} \int k_I q_i dq_i + \sum_{i=n+1}^{2n} \int k_{II} q_i dq_i$. The structural stiffness expressed in Nm/rad is defined as $k_I = \sum_{j=0}^{b} k_j |\theta|^{jr} > 0$ on the bending plane and as $k_{II} = \sum_{j=0}^{b} k_j |\omega|^{jr} > 0$ in the direction orthogonal to the bending plane. The constant parameters $b > 0$, $0 < r < 1$, and $k_j > 0$ are known, while $\theta = \sum_{i=1}^{n} q_i$, and $\omega = \sum_{i=n+1}^{2n} q_i$. The relationship between k_j in Nm/rad and k_j^* in bar/rad depends on the geometry of the manipulator. For a prototype with a circular section of diameter D and three equal internal chambers with thin partition walls as shown in Figure 1 we have $k_j \cong k_j^* \pi D^3/24$.

Assumption 3: The physical damping is defined by the matrix $R_I = \left(R_0 + R_1 \left|\dot{\theta}\right|^2\right) I$ on the bending plane, and by the matrix $R_{II} = (R_0 + R_1 |\dot{\gamma}|^2) I$ in the direction orthogonal to the bending plane, where $R_0 > 0, R_1 > 0$ are known constants.

Assumption 4: The disturbance does not include twisting effects and is commensurate with the ultimate strength of the material so that no plastic deformation or rupture occurs. As a result, an arbitrary disturbance δ corresponds to a set of attainable equilibria q^* that verify the condition

$$G^{\perp}\left(\nabla_q V(q^*) + \delta\right) = 0, \tag{4}$$

where the matrix $G^{\perp}$ is such that $G^{\perp} G = 0$ and $\mathrm{rank}\{G^{\perp}\} = 2n - 1$. Equation (4) is obtained by computing (3) at the equilibrium (i.e. setting $\dot{q} = p = \dot{p} = 0$) and by pre-multiplying it by $G^{\perp}$, thus it is generally valid, and it defines a set of equilibrium points for the unactuated DOFs.

Assumption 5: The time-varying disturbance δ is unknown and bounded, thus $\underline{\Delta} \leq \delta \leq \overline{\Delta}$ for some unknown values $\underline{\Delta}$ and $\overline{\Delta}$ such that $\underline{\Delta} \leq \overline{\Delta}$, with $l = \left(\underline{\Delta} + \overline{\Delta}\right)/2$ constant and unknown. The time-varying component of the disturbance is $\sigma = \delta - l$, with $|\sigma| \leq \varepsilon$, where the bound $\varepsilon \in \mathbb{R}^{2n+1}$ is constant and known. Additionally, $|\sigma| \leq \mu |\dot{q}|$ for some known $\mu > 0$.

Note that no elastic energy is associated to the position $q_{2n+1} = \varphi$ since the latter depends only on the geometry of the internal chambers and on the corresponding pressures. The weight of the manipulator is not accounted for explicitly in the potential energy but instead it is treated as a disturbance thus the control law does not depend on the orientation of the base frame with respect to gravity. *Assumption 2* implies that stiffness is uniform along the length, which is reasonable if the manipulator has a constant section. This approach provides a convenient approximation of the potential energy of the manipulator and allows identifying the stiffness parameters from experimental data since the tip rotation is directly measurable (see Section IV). Approximating the load-deflection relationship of a compliant structural element with a polynomial has originally been proposed as part of the pseudo-rigid-body model approach [37]. Polynomial approximations have also been employed for the curvature of soft continuum

manipulators in [23]. Conversely, identifying non-uniform stiffness parameters would require a more complex setup and a larger number of sensors. Since damping in pneumatic systems is nonlinear, it is approximated with a polynomial model [38]. The effect of these approximations is lumped in the disturbance δ, which is decomposed into an unknown constant term and a time-varying bounded term similarly to [33]. Finally, no assumption is made on the mass of the manipulator for the purpose of the stability analysis. This is a further difference from our preliminary results [30] which only consider manipulators with total mass $m_T \ll 1$ in an attempt to conclude the existence of local stability conditions. This limitation is removed in the present work and stability conditions are provided in *Proposition 1*. In addition, the case $m_T \ll 1$ is discussed separately in *Remark 1* and the respective stability conditions are expressed in closed form.

III. Controller Design

The control objective consists in stabilizing the prescribed equilibrium point $(\theta,\gamma)=(\theta_d,\gamma_d)$ in spite of the unknown external disturbances and of the model uncertainties, while only relying on the values of $\theta,\dot{\theta},\gamma$, and $\dot{\gamma}$ at any instant.

A. Energy shaping control

The proposed control approach is based on an extension of the IDA-PBC formulation [30], [39]. Accordingly, the closed-loop dynamics in port-Hamiltonian form is representative of a mechanical system with total energy W and is expressed as

$$\begin{bmatrix}\dot{q}\\ \dot{p}\end{bmatrix}=\begin{bmatrix}0 & M^{-1}M_d\\ -M_dM^{-1} & J_2-R_d\end{bmatrix}\begin{bmatrix}\nabla_q W\\ \nabla_p W\end{bmatrix}-\begin{bmatrix}0\\ \sigma\end{bmatrix}+\begin{bmatrix}0\\ G\end{bmatrix}u_0, \quad (5)$$

where $W=H_d+\Lambda^T(q-q^*)+\mathcal{C}$, and $\mathcal{C}>0$ is a constant ensuring $W>0$. The free matrix $J_2=-J_2^T$ depends on p, and the closed-loop damping is $R_d=Gk_vG^T+RM^{-1}M_d$, where $k_v=k_v^T>0$ is a tuning parameter. The ancillary control u_0 is designed to mitigate the effect of σ, as discussed in Section III.B. The new Hamiltonian $H_d=\frac{1}{2}p^TM_d^{-1}p+V_d$ represents the mechanical energy of the closed-loop system, $\Lambda^T(q-q^*)$ accounts for the work of the constant disturbances $G^\perp l$ affecting the unactuated DOFs, and the term Λ can be interpreted as a vector of closed-loop non-conservative forces. Consequently, $\nabla_pW=\nabla_pH_d$, while $\nabla_qW=\nabla_qH_d+\Lambda$. The kinetic energy $T_d=\frac{1}{2}p^TM_d^{-1}p$ with inertia matrix $M_d=M_d^T>0$, and the potential energy V_d are the main design parameters in the energy shaping procedure. To achieve the regulation goal $q=q^*$ the total energy W is designed to have a strict minimizer at the prescribed equilibrium position, that is $q^*=\mathrm{argmin}(W)$. Since the system is underactuated, the control input cannot be computed by equating (3) and (5) and by inverting G. Instead, the terms V_d, M_d and J_2 should satisfy the following set of partial differential equations (PDEs) [27]

$$G^\perp\left(\nabla_qT-M_dM^{-1}\nabla_qT_d+2J_2M_d^{-1}p\right)=0, \quad (6.a)$$

$$G^\perp\left(\nabla_qV-M_dM^{-1}\nabla_qV_d\right)=0, \quad (6.b)$$

and Λ should satisfy the $2n-1$ algebraic equations

$$G^\perp(l-M_dM^{-1}\Lambda)=0. \quad (7)$$

Provided (6) are solvable and V_d and M_d can be expressed analytically in closed form, the IDA-PBC control law that applied to (3) yields the closed-loop dynamics (5) is thus

$$\begin{gathered}u=u_{es}+u^*+u_0\\ u_{es}=G^\dagger\left(\nabla_qH-M_dM^{-1}\nabla_qH_d\right)+(G^\dagger J_2-k_vG^T)\nabla_pH_d\\ u^*=G^\dagger(l-M_dM^{-1}\Lambda),\end{gathered} \quad (8)$$

where $G^\dagger=(G^TG)^{-1}G^T$ is the pseudo-inverse of G. Defining $M_d=k_mM$, where $k_m>0$ is a constant tuning parameter, verifies (6.a) with $J_2=0$ and scales the open-loop kinetic energy T by a factor k_m. Substituting M_d in (8) removes the kinetic terms ∇_qT, ∇_qT_d and ensures closed-loop dissipation for all $k_v=k_v^T\geq 0$ since $R_d=(Gk_vG^T+Rk_m)>0$ [34].

The candidate solution of the potential-energy PDE (6.b) is

$$\begin{aligned}V_d=&\frac{k_0}{2k_m}\sum_{i=1}^{n}q_i^2-\frac{k_0}{2nk_m}\theta^2+\frac{k_p}{2k_m}(\theta-\theta_d)^2\\ &+\frac{1}{k_m}\sum_{i=n+1}^{2n}\int k_{II}q_i\,dq_i+\frac{k_p}{2k_m}(\gamma-\gamma_d)^2,\end{aligned} \quad (9)$$

where $k_p>0$ is a further tuning parameter. In particular, (9) accounts for the nonlinear stiffness of the model, it verifies (6.b) for all θ and for $\gamma=\gamma_d$, and it is defined such that $(\theta_d,\gamma_d)=\mathrm{argmin}(V_d)$. In order for W to also have a strict minimizer at the equilibrium $(\theta,\gamma)=(\theta_d,\gamma_d)$, the conditions

$$\nabla_qW(q^*,0)=\nabla_qV_d(q^*)+\Lambda=0, \quad (10.a)$$

$$\nabla_q^2V_d=\frac{nk_0^{n+1}k_p^2}{k_m^{n+4}}\left(k_0+\sum_{j=1}^{b}s_jrk_j|\omega|^{jr}\right)>0, \quad (10.b)$$

should be met, where s_j are positive constants that depend on r and j (e.g. $s_1=3$ and $s_2=9$ if $r=4/5$). Solving (7) for a disturbance estimate $\hat{l}$ to be defined in Section III.B, while also verifying (10.a), yields a constant vector Λ of elements

$$\Lambda_i=\begin{cases}\frac{1}{n}\left(\frac{(n-1)\hat{l}_i}{k_m}-\sum_{j=1}^{n}\frac{\hat{l}_{j\neq i}}{k_m}\right) & 1\leq i\leq n,\\ \hat{l}_i/k_m & n+1\leq i\leq 2n.\end{cases} \quad (11)$$

Since Λ is constant, it does not appear in inequality (10.b), which is verified for all $k_p>0$ and $k_m>0$. Substituting (9) and (11) into (8) yields the IDA-PBC control law

$$\begin{bmatrix}u_I\\ u_{II}\end{bmatrix}=\begin{bmatrix}\frac{1}{n}\sum_{j=0}^{b}k_j|\theta|^{jr+1}-k_p(\theta-\theta_d)-\frac{k_{vI}}{k_m}\dot{\theta}\\ -k_p(\gamma-\gamma_d)-\frac{k_{vII}}{k_m}\dot{\gamma}\end{bmatrix}+u^*+u_0, \quad (12)$$

where $k_v=\mathrm{diag}(k_{vI},k_{vII})$ and u_0 is defined in Section III.B. In addition, $u^*=G^\dagger\hat{l}$ since $G^\dagger k_m\Lambda=0$. This last simplification is due to the structure of (11) and to the choice

$M_d = k_m M$. Local stability of the equilibrium is concluded for constant disturbances $\delta = l$ using a similar approach to our preliminary work [30]. The more realistic case of unknown time-varying disturbances is studied in the next Section.

B. Disturbance Rejection

The estimate of the unknown constant disturbance $G^\dagger \hat{l}$ appearing in (12) is computed here with a modification of the I&I method [32] resulting in the adaptive law

$$\dot{\hat{l}} = -\alpha\big(\nabla_q V + R\dot{q} - Gu + \hat{l}\big), \tag{13}$$

where $\alpha > 0$ is a constant tuning parameter. Additionally, to mitigate the effect of σ we define the ancillary control u_0 as

$$u_0 = -\bar{\varepsilon}\begin{bmatrix}\tanh(\dot{\theta})\\ 0\end{bmatrix}, \tag{14}$$

where $\bar{\varepsilon} = \max(\varepsilon)$ is a known parameter (see *Assumption 5*). Note that u_0 only contributes to u_I, which acts on the bending plane (see *Remark 2*). Substituting (12) into (13) and pre-multiplying by $G^\dagger$ yields the adaptive law in explicit form

$$G^\dagger \dot{\hat{l}} = -\alpha\begin{bmatrix} k_p(\theta - \theta_d) + \dfrac{k_{vI}}{k_m}\dot{\theta} + \dfrac{1}{n}R_I\dot{\theta} + \bar{\varepsilon}\tanh(\dot{\theta}) \\ k_p(\gamma - \gamma_d) + \dfrac{k_{vII}}{k_m}\dot{\gamma} + R_{II}\dot{\gamma}\end{bmatrix}. \tag{15}$$

Computing u^* by integrating (15) in time and substituting it into (12) yields the complete control law

$$u_I = \frac{1}{n}\sum_{j=0}^{b} k_j|\theta|^{jr+1} - k_p(\theta - \theta_d) - \frac{k_{vI}}{k_m}\dot{\theta} - \bar{\varepsilon}\tanh(\dot{\theta}) + \alpha\int_0^t\left(-k_p(\theta - \theta_d) - \frac{k_{vI}}{k_m}\dot{\theta} - \frac{R_I}{n}\dot{\theta} - \bar{\varepsilon}\tanh(\dot{\theta})\right)d\tau, \tag{16.a}$$

$$u_{II} = \alpha\int_0^t\left(-k_p(\gamma - \gamma_d) - \frac{k_{vII}}{k_m}\dot{\gamma} - R_{II}\dot{\gamma}\right)d\tau - k_p(\gamma - \gamma_d) - \dot{\gamma}\,k_{vII}/k_m\,, \tag{16.b}$$

which is nonlinear and implementable since it only depends on $\theta, \gamma, \dot{\theta}$, $\dot{\gamma}$, and on the model parameters as initially required. Employing a similar argument as [21] shows that the integral terms in (16) do not add to the stiffness of the manipulator in closed loop, which is confirmed by the expression of V_d (9).

Proposition 1: Consider system (3) with *Assumptions 1* to *5* in closed-loop with the controller (16). Define the vector of estimation errors as $z = \hat{l} - \alpha p - l$. Define the positive tuning parameters k_{vI}, k_{vII}, α, and k_m such that $\mathcal{A} > 0$ and $\mathcal{B} > 0$ (see Appendix). Then the following claims hold.

i) The equilibrium point $(q, p, z) = (q^*, 0, 0)$ is locally stable and q converge asymptotically to the set q^* defined in (4).
ii) The point (θ_d, γ_d) is a strict minimizer of W for all $k_p > 0$ thus (θ, γ) converge to (θ_d, γ_d) asymptotically.

Proof: To prove the first claim we start by computing the time derivative of z and by substituting (3), which gives

$$\dot{z} = \dot{\hat{l}} + \alpha\big(\nabla_q H + R\nabla_p H - Gu + \hat{l} - \alpha p - z - \sigma\big). \tag{17}$$

Substituting the adaptive law (13) into (17) gives

$$\dot{z} = \alpha\big(\nabla_q(p^T M^{-1} p)/2 \; - \alpha p - z - \sigma\big). \tag{18}$$

Since (18) also contains terms depending on p, the dynamics of z is studied together with that of the closed-loop system (5). Substituting $M_d = k_m M$ and $J_2 = 0$ in (5) and computing the time derivative of W gives

$$\dot{W} = \nabla_p H_d^T\big(-(Gk_vG^T + Rk_m)\nabla_p H_d + G(u_0 + u^*) - \delta\big). \tag{19}$$

Defining the Lyapunov function candidate $W' = W + \frac{1}{2}z^T z$, computing its time derivative along the trajectories of the closed-loop system, and substituting (16),(18),(19) while indicating with $[1_n^T]$ the column vector of dimension n yields

$$\begin{aligned}\dot{W}' = &-\big(k_{vI}\dot{\theta}^2 + k_{vII}\dot{\varphi}\dot{\gamma}\big)\frac{1}{k_m^2} - |\dot{q}|^2\frac{R}{k_m} + \\ &+\frac{\dot{q}^T}{k_m}\Big(z + \alpha p + \sigma - [1_n^T]\bar{\varepsilon}\tanh(\dot{\theta})\Big) - \alpha z^T z + \\ &+\alpha z^T\big(\nabla_q(p^T M^{-1} p)/2 \; - \alpha p - \sigma\big).\end{aligned} \tag{20}$$

For the rigid-link model we have that $\lambda_{\mathrm{MAX}}\{M\} \le m_T L_T^2$, where m_T and L_T are the total mass and the total length of the manipulator, and the operator $\lambda_{\mathrm{MAX}}\{\cdot\}$ indicates the largest eigenvalue of a matrix. As a result, $|p| \le c_1 m_T L_T^2|\dot{q}|$ and $\big|\nabla_q(p^T M^{-1} p)\big|/2 \le c_2 m_T L_T^2|\dot{q}|^2$ for some $0 < c_1 \le 1$ and $0 < c_2 \le 1/2$, which substituted in (20) yields

$$\begin{aligned}\dot{W}' \le &-\big(k_{vI}\dot{\theta}^2 + k_{vII}\dot{\varphi}\dot{\gamma}\big)\frac{1}{k_m^2} - |\dot{q}|^2\left(\frac{R_0 - \alpha c_1 m_T L_T^2}{k_m}\right) + \\ &+|z||\dot{q}|\left(\frac{1}{k_m} + \alpha^2 c_1 m_T L_T^2\right) + |z||\dot{q}|^2(\alpha c_2 m_T L_T^2) + \\ &-|\dot{q}|^4\frac{R_1}{k_m} - \alpha|z|^2 - \frac{\bar{\varepsilon}}{k_m}\dot{\theta}\tanh(\dot{\theta}) + \frac{|\dot{q}||\sigma|}{k_m} + \alpha|z||\sigma|.\end{aligned} \tag{21}$$

Using the Cauchy-Schwarz inequality $\sum_{i=1}^n \dot{q}_i^2 \ge (\sum_{i=1}^n \dot{q}_i)^2/n$ yields $|\dot{q}|^2 \ge \frac{\dot{\theta}^2}{n} + \dot{\varphi}^2 + \frac{\dot{\omega}^2}{n}$. Substituting the former inequality in (21) and recalling that $\gamma = \omega + \varphi$ gives

$$\begin{aligned}\dot{W}' \le &-\frac{k_{vII}}{k_m^2}(\dot{\varphi}^2 + \dot{\varphi}\dot{\omega}) - \left(\frac{\dot{\theta}^2}{n} + \dot{\varphi}^2 + \frac{\dot{\omega}^2}{n}\right)\frac{R_0}{2k_m} \\ &-\frac{k_{vI}}{k_m^2}\dot{\theta}^2 - |\dot{q}|^2\left(\frac{R_0}{2k_m} - \frac{\alpha c_1 m_T L_T^2}{k_m}\right) - |\dot{q}|^4\frac{R_1}{k_m} - \alpha|z|^2 + \\ &+|z||\dot{q}|\left(\frac{1}{k_m} + \alpha^2 c_1 m_T L_T^2\right) + |z||\dot{q}|^2(\alpha c_2 m_T L_T^2) - \\ &-\frac{\bar{\varepsilon}}{k_m}\dot{\theta}\tanh(\dot{\theta}) + \frac{|\dot{q}||\sigma|}{k_m} + \alpha|z||\sigma|.\end{aligned} \tag{22}$$

Rearranging terms in (22), defining $x = [|\dot{q}| \quad |\dot{q}|^2 \quad |z|]$, and substituting $|\sigma| \le \mu|\dot{q}|$ from *Assumption 5* yields

$$\begin{aligned}\dot{W}' \le &-\dot{\theta}^2\left(\frac{k_{vI}}{k_m^2} + \frac{R_0}{2nk_m}\right) - [\dot{\varphi} \quad \dot{\omega}]\mathcal{A}\begin{bmatrix}\dot{\varphi}\\ \dot{\omega}\end{bmatrix} \\ &-x\,\mathcal{B}\,x^T - \frac{\bar{\varepsilon}}{k_m}\dot{\theta}\tanh(\dot{\theta}),\end{aligned} \tag{23}$$

with $\mathcal{A}$ and $\mathcal{B}$ defined in Appendix, and where the last term is

negative semidefinite and is due to u_0. From (23), we have that $\dot{W}' \leq 0$ if $\mathcal{A} > 0, \mathcal{B} > 0$. As a result, $\dot{q} \in \mathcal{L}_2 \cap \mathcal{L}_\infty$, while computing $\dot{p}$ from (5) yields $\dot{p} \in \mathcal{L}_\infty$. Similarly, $z \in \mathcal{L}_2 \cap \mathcal{L}_\infty$, and $\dot{z} \in \mathcal{L}_\infty$ from (18). Thus p and z are bounded and converge to zero asymptotically by Barbalat's Lemma. Substituting $p = \dot{q} = \dot{p} = 0$ in (5) gives $\nabla_q V_d + \Lambda = 0$, which corresponds to (10.a), thus q converges to q^* proving claim i).

To prove the second claim we observe that q^* is a strict minimizer of W for all $k_p > 0$ from (10.b). Thus, we only need to prove that the regulation goal $(\theta, \gamma) = (\theta_d, \gamma_d)$ belongs to the set of attainable equilibria q^* defined in (4). Computing (4) with $\sigma = 0$ (see *Assumption 5*) yields

$$\begin{cases} (q_i - q_n)k_I = \hat{l}_n - \hat{l}_i & 1 \leq i < n, \\ q_i k_{II} = -\hat{l}_i & n+1 \leq i \leq 2n, \end{cases} \tag{24}$$

where q_n and q_{2n+1} can be chosen such that

$$(nq_n - \theta_d)k_I = -(n-1)\hat{l}_n + \sum_{i=1}^{n-1} \hat{l}_i, \tag{25.a}$$

$$(q_{2n+1} - \gamma_d)k_{II} = \sum_{i=n+1}^{2n+1} \hat{l}_i. \tag{25.b}$$

Computing $\theta = \sum_{i=1}^{n} q_i$ and $\gamma = \sum_{i=n+1}^{2n+1} q_i$ from (24) and (25) yields $(\theta, \gamma) = (\theta_d, \gamma_d)$ thus proving claim ii) ■

Remark 1: Differently from our preliminary results [30], the control law (16) accounts for the nonlinear structural stiffness of the manipulator and includes the nonlinear damping term (14). In addition, the control input u_2^* accounts for the effect of damping in the direction orthogonal to the bending plane, thus leading to a gradual and smooth convergence of γ to γ_d (see Section IV). Additionally, *Proposition 1* provides explicit stability conditions which refer to the tuning parameters and to the physical damping. This is a much stronger result compared to [30], which only concludes the existence of local stability conditions, depending on the estimation error z, without providing tuning guidelines. While closed-loop dissipation is ensured for all $k_{vI} \geq 0$ and $k_{vII} \geq 0$, inequality (A4) prescribes an upper limit on k_{vII} that decreases with n and is proportional to $R_0 k_m$. The value of k_{vII} can be kept constant for larger n if the parameter k_m is also increased, which corresponds to prescribing larger closed-loop inertia. If $m_T L_T^2 \ll 1$, which is typically the case for miniature soft continuum manipulators such as [36] and for similar designs such as [35], the condition $\mathcal{B} > 0$ can be approximated as

$$R_0 - 2\mu + 2\alpha k_m - 2\sqrt{\Xi} > 0, \tag{26.a}$$

$$R_1/k_m > 0, \tag{26.b}$$

where the term Ξ does not depend on R_1 and it is defined as

$$\Xi = \frac{R_0^2}{4} + (4\mu - R_0)\alpha k_m - R_0\mu + (\alpha^2 k_m^2 + 1)(\mu^2 + 1). \tag{27}$$

Inequality (26.b) is verified since $R_1 > 0$ by hypothesis, hence nonlinear damping is instrumental to stability. The tuning guidelines for α and k_m corresponding to inequality (26.a) are

$$\begin{gathered} \left(R_0 - 3\mu - \sqrt{\varrho}\right)/\mu^2 < \alpha k_m < \left(R_0 - 3\mu + \sqrt{\varrho}\right)/\mu^2, \\ \varrho = R_0^2 + 8\mu^2 - 6R_0\mu > 0, \\ R_0 > 3\mu. \end{gathered} \tag{28}$$

Solving (28) for $\mu = \lambda R_0$ yields $\lambda \leq 1/4$ thus a larger physical damping R_0 is required to withstand the effect of larger time-varying disturbances. Computing (28) for the limit condition $\mu = R_0/4$ yields $\alpha k_m = 4/R_0$, thus a larger physical damping demands a less aggressive tuning of the adaptive law or a smaller k_m. Additionally, in case of pneumatic actuation, R_0 can be increased as needed by introducing flow restrictors on the lines that supply the manipulator, resulting in a smoother but slower transient response (see Section IV). Note that the tuning guidelines (28) are conservative since the Cauchy-Schwarz inequality is used in (22), hence they ensure stability of the desired equilibrium. However compared to *Corollary 1* in [29], the conditions (28) are less stringent (see Section IV.A for a numerical example).

In summary, (16) contains the tuning parameters k_p, k_{vI}, k_{vII}, α, k_m, and $\overline{\varepsilon}$ which is assumed known (see *Assumption* 5). In particular, α defines the convergence rate of the adaptive law (15), thus a larger value is typically desirable compatibly with (28). In addition, k_m, k_{vI}, k_{vII} appear in (16) as k_{vI}/k_m and k_{vII}/k_m, thus they can be treated as two parameters: k_{vII}/k_m should verify (A4); k_{vI}/k_m can be taken of the same order of magnitude as R_0 to start with, and further reducing its value results in a faster response. Employing a larger k_p results in a faster transient but also increases the closed-loop stiffness, which is typically undesirable for soft continuum manipulators [21]. In this respect, values in the range $k_0/10 < k_p < k_0/3$ represent a good compromise. The effect of the tuning parameters is illustrated in Section IV.

Remark 2: The ancillary control (14) only affects the bending plane thus the product $\nabla_p H_d^T G u_0$ in (19) provides a negative-semidefinite contribution in (23). For illustrative purposes, defining $u_0' = -\overline{\varepsilon}\begin{bmatrix}\tanh(\dot{\theta}) \\ \tanh(\dot{\gamma})\end{bmatrix}$ and substituting it in (23) yields $\dot{W}'' = \dot{W}' - \overline{\varepsilon}\dot{\varphi}\tanh(\dot{\gamma})/k_m$, where in general the last term has indeterminate sign. Although this additional term could be accounted for the in the matrix $\mathcal{A}$ by employing the Cauchy-Schwarz inequality as outlined in (22), it would result in more stringent stability conditions. Consequently u_0 is defined such that it only contributes to the in-plane control u_I.

Remark 3: The model of the structural stiffness defined in *Assumption 2* is instrumental to ensuring that an analytical solution of (6.b) exists for all θ and $\gamma = \gamma_d$, and that the control law (16) is implementable by employing only the tip angles θ and γ and their first order time derivatives. *Assumption 2* would not be satisfied by soft manipulators with non-uniform stiffness (e.g. $k_i = \sum_{j=0}^{b} k_{ij}|q_i|^{jr}$ different for each joint i, where $1 \leq i \leq 2n$). In such a case, an additional state observer would be required to estimate the virtual positions q_i that would appear in the control law. In addition, the theoretical case of nonlinear uniform stiffness with $k_0 = 0$

is also problematic since the PDE (6.b) would then only be solvable for the CC condition $q_i = q_j, \forall i,j$. This implies that the closed-loop dynamics would correspond to (5) only in proximity of the equilibrium q^* and only if the disturbance does not affect the unactuated DOFs [29], thus resulting in degraded transient performance. The latter case is less relevant in practice since it would imply that the structural stiffness is zero at $\theta = 0$, which might not be physically meaningful. Instead, the case of non-uniform stiffness could be relevant to soft manipulators with variable section along their axis and shall be investigated as part of our future work.

IV. Experimental Results

A. Simulations

Simulations have been conducted in Matlab for the rigid-link model shown in Figure 1 with the parameters $n = 3$, $k_0 = 2$, $k_1 = 4$, $b = 1$, $r = 0.25$, $l_T = 0.1$, $m_T = 1.5$, $R_0 = 0.01$, $R_1 = 0.0001$. The disturbances have been defined as $\delta = l + \sigma$, with a constant part $l = -0.01[5\ 5\ 5\ 0\ 0\ 0\ 5]$, where the first three terms represent moment loads in the bending plane, the next three terms are moment loads outside the bending plane, and the last term can be due to asymmetries in the internal chambers of the manipulator. The variable component of the disturbance changes suddenly from $\sigma = 0$ to $\sigma = -0.01[5\ 5\ 5\ 5\ 5\ 5\ 5]$ at time $t = 2.5$ seconds and represents an additional moment load in the bending plane and a further moment that moves the manipulator away from the bending plane. Consequently, $\varepsilon = 0.05$ and $\mu = 0$ since the disturbance does not include damping terms. Computing (A4) and (28) while assuming $\mu = R_0/5$ for illustrative purposes results in the tuning guidelines $k_{vII} < 0.05$ and $27 \leq \alpha k_m \leq 373$, while the limit condition $\mu = R_0/4$ corresponds to $\alpha k_m = 400$ (see *Remark 1*). In comparison, the tuning guidelines in *Corollary 1* [29] for the planar case with $\mu = 0$ would be $32 \leq \alpha k_m \leq 192$, which are more restrictive. The controller parameters are finally chosen as $k_{vI} = 0.1$, $k_{vII} = 0.15$, $k_p = 0.2$, $\alpha = 10$, $k_m = 5$ and alternatively $k_m = 10$.

The effect of the tuning parameters α, k_p and $\bar{\varepsilon}$ is shown in Figure 2. The effect of the tuning parameters k_m, k_{vI}, k_{vII} and of the stiffness parameters k_I, k_{II} is shown in Figure 3. Figure 2 shows that the controller (16) achieves the regulation goal in spite of the disturbances. After the disturbance onset, the control input settles at a higher value because of the adaptive law (15). The disturbance estimates $G^T\hat{l}$, consisting of the in-plane component $\hat{l}_I$ and of the out-of-plane component $\hat{l}_{II}$, converge to $G^T(l+\sigma)$ (see Figure 2.c and 2.f). Employing $\bar{\varepsilon} = 0.05$ results in a slower transient but also in a smaller deviation of the tip angle θ from the desired value θ_d immediately after $t = 2.5$ seconds compared to the case in which $\bar{\varepsilon} = 0$. Instead, the time history of the tip angle γ is the same in both cases, since u_0 only affects the control law u_I (see *Remark 2*). Increasing α leads to a faster recovery from the disturbance and preserves the transient for both θ and γ. Instead, increasing k_p result in a faster transient and also leads to overshoot and oscillations on γ (see *Remark 1*).

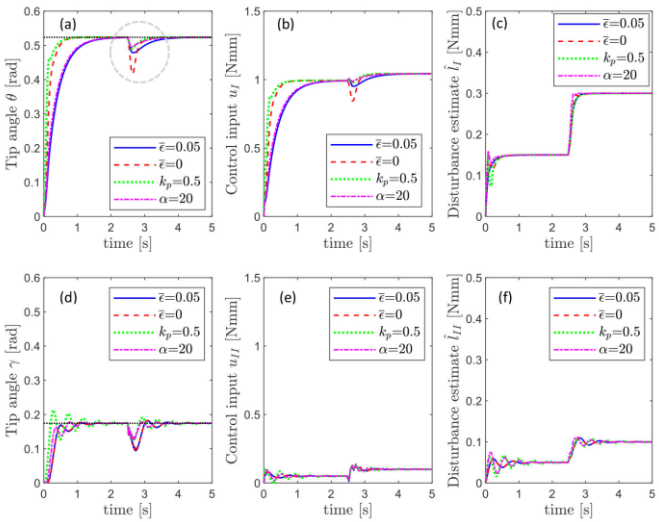

Figure 2. Simulation results with $k_m = 5$ and different values of $\alpha, k_p, \bar{\varepsilon}$: tip angle θ (a); tip angle γ (d); control input u_I (b); control input u_{II} (e); disturbance estimate $\hat{l}_I$ (c); disturbance estimate $\hat{l}_{II}$ (f). The tuning parameters of controller (16) are $k_{vI} = 0.1$, $k_{vII} = 0.15$, $k_p = 0.2$, $\alpha = 10, \bar{\varepsilon} = 0.05$ unless otherwise stated in the legend.

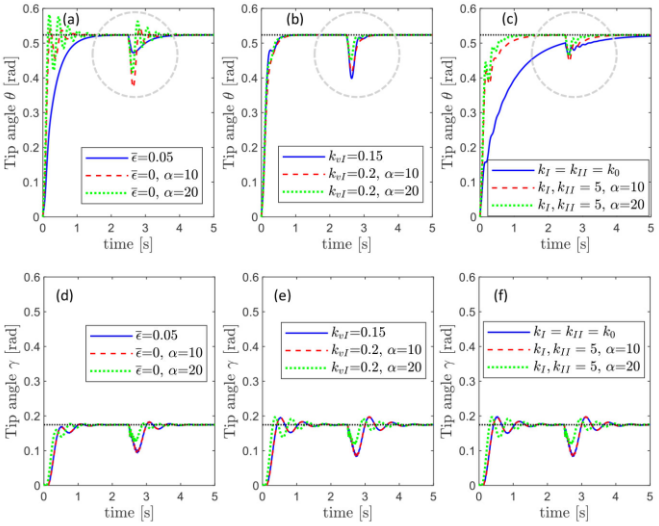

Figure 3. Simulation results with $k_m = 10$ and different values of $\alpha, k_{vI}, \bar{\varepsilon}$: tip angle θ (a); and tip angle γ (d); tip angle θ with $u_0 = 0$ (b); and tip angle γ with $u_0 = 0$ (e); tip angle θ for our previous implementation [29], [30] (c); and tip angle γ (f). The tuning parameters are $k_{vI} = 0.1, k_{vII} = 0.15, k_p = 0.2, \alpha = 10, \bar{\varepsilon} = 0.05, k_m = 10$ in (16), unless otherwise stated in the legend.

Figure 3.a shows that increasing k_m results in a faster transient but might induce overshoot and oscillations if $\bar{\varepsilon} = 0$. A smoother but slower response is obtained with $\bar{\varepsilon} = 0.05$ and the system recovers from the disturbance in a similar way as shown in Figure 2.a. Introducing the nonlinear term u_0 has a different effect compared to simply increasing the parameter k_{vI} of an equal amount, as shown by Figure 3.b. Further increasing k_{vI} recovers a similar response to the disturbance but at the cost of a slower transient. Employing a constant stiffness parameter $k_I = k_{II} = k_0$ and $\bar{\varepsilon} = 0$ in the control law as in our earlier works [29], [30] results in a slower transient since the adaptive law has to compensate for the discrepancy between the estimated value and the actual value of the structural stiffness (see Figure 3.c). This issue can be partially

mitigated by employing a larger k_0 in the control law, which however needs to be chosen according to the operating conditions to maximize responsiveness while avoiding overshoot and oscillations. Increasing α can result in a faster response but used in conjunction with a large k_m it could also lead to a more oscillatory transient (see *Remark 1*). Finally, setting $\alpha = 0$ deactivates the adaptive law thus the control input does not change after the disturbance onset leading to a large steady-state error $(\theta_d - \theta, \gamma_d - \gamma) = (0.5, 0.58)$.

B. Experiments

The controller (16) has been tested on a prototype with outer diameter $D = 6$ mm, total length $l_T = 30$ mm, and total mass $m_T = 1.5$ g employing the setup illustrated in Figure 1.e. The tip angles (θ, γ) are measured with an electromagnetic tracking system (Aurora, NDI, Canada, 0.2° RMS accuracy for 5DOF sensor) and are communicated to a Matlab script. The control pressures are computed from (2) and are communicated to two proportional pressure regulators (Tecno Basic, Hoerbiger, Germany) using a digital microcontroller (mbed NXP LPC1768, baud rate 921600). The pressure regulators supply two chambers of the manipulator, while the third chamber is left at atmospheric pressure for simplicity. Pressurizing the third chamber results in different values of φ.

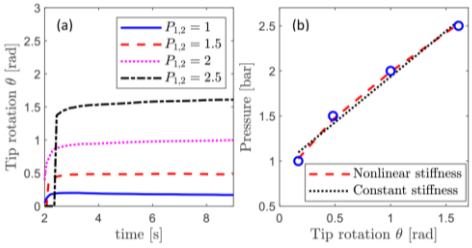

Figure 4. Tip rotation of the manipulator on the bending plane for different values of the actuation pressures $P_1 = P_2$ (a); least-squares regression for the stiffness parameters k_j^* compared to constant stiffness approximation (b).

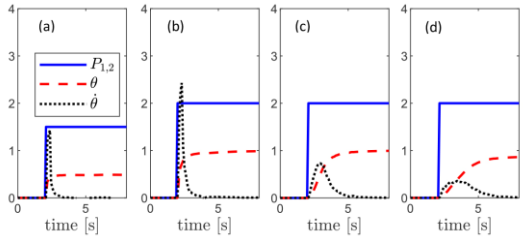

Figure 5. Step response of the manipulator with $P_0 = 0, P_1 = P_2 = 1.5$ bar (a); with $P_1 = P_2 = 2$ bar (b); with $P_1 = P_2 = 2$ bar and flow restrictor (3 mm ID) half open (c); $P_1 = P_2 = 2$ bar and flow restrictor a quarter open (d).

Physical damping and structural stiffness parameters have been estimated with a set of step responses of different amplitudes. Figure 4 shows that the tip rotation θ increases with the input pressure. The measurements have been conducted setting different values of $P_1 = P_2$ and keeping $P_0 = 0$. Defining $\vartheta = \theta^r$ and employing a least-squares regression in ϑ yields $k_l^* = k_0^* + k_1^* |\theta|^r$ expressed in bar/rad. The values $k_0^* = 0.6$, $k_1^* = 1.3$, and $r = 0.25$ represent a good approximation for this range of pressures and provide better accuracy than assuming constant stiffness (see Figure 4.b), which is even more noticeable over a larger pressure range.

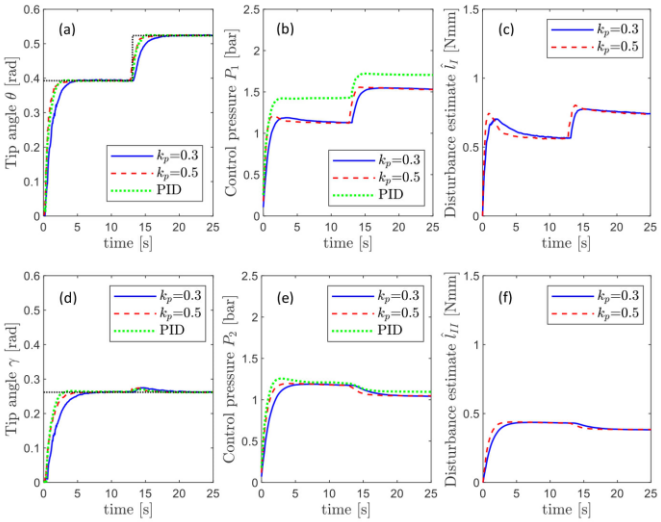

Figure 6. Experimental results without external forces (test setup in Figure 1.e): time histories of the tip angle θ (a); tip angle γ (d); control pressure P_1 (b); control pressure P_2 (e); disturbance estimate $\hat{l}_I$ (c); disturbance estimate $\hat{l}_{II}$ (f). The tuning parameters of controller (16) are $k_p = 0.5, k_{vI} = k_{vII} = 1, k_m = 20, \alpha = 10$, and $\bar{\varepsilon} = 0.05$ unless otherwise stated in the legend.

The structural stiffness in Nmm/rad is computed considering a circular section thus $k_j = k_j^* \pi D^3/24$, which yields $k_0 = 1.7$, $k_1 = 3.7$. Figure 5.a and 5.b show that the maximum angular speed $\dot{\theta}$ varies at different pressures, which indicates the presence of nonlinear damping. The experiments have also confirmed that damping can be substantially increased by introducing a flow restrictor at the output of the pressure regulators (see Figure 5.c and 5.d). The damping parameters have been estimated from (3) computed at the maximum velocity for different actuation pressures without external forces. In these conditions the manipulator admits a constant-curvature equilibrium thus $q_i = q_j$ for all i and j. The tip rotation θ, the velocity $\dot{\theta}$, and the control input are known at any instant. The damping parameters resulting from the model identification are $R_0 = 3 \times 10^{-2}$ Nms and $R_1 = 1.5 \times 10^{-2}$Nms^2 thus the physical damping on the bending plane has been modelled as $R_I = R_0 + R_1 \dot{\theta}^2$. Computing (28) while assuming $\mu = R_0/5$ for illustrative purposes, as in the simulations, results in the tuning guidelines $45 < \alpha k_m < 620$, while the limit condition $\mu = R_0/4$ yields $\alpha k_m = 133$. The tuning parameters have been set to $k_p = 0.5$; $k_{vI} = k_{vII} = 1; k_m = 20$; $\alpha = 10$, and $\bar{\varepsilon} = 0.05$. This represents a more aggressive tuning of α and k_m compared to the limit condition $\mu = R_0/4$, which is conservative (see *Remark 1*). These values have been chosen to facilitate the comparison with our prior work and since the external forces in the experiments do not include damping terms, thus $\mu \cong 0$. Since a different parameterization has been used for the potential energy V_d in (9), the parameter k_p in (16) corresponds to the product $k_p k_m$ in [29], thus the controller parameters are equivalent in both cases. For comparison purposes, the system response is also shown for a PID algorithm with tuning parameters $K_p = k_p = 0.5$, $K_i = \alpha k_p = 5$ and $K_d = k_{vI}/k_m = 1/20$. Further experiments with the PID can be found in our prior work [29].

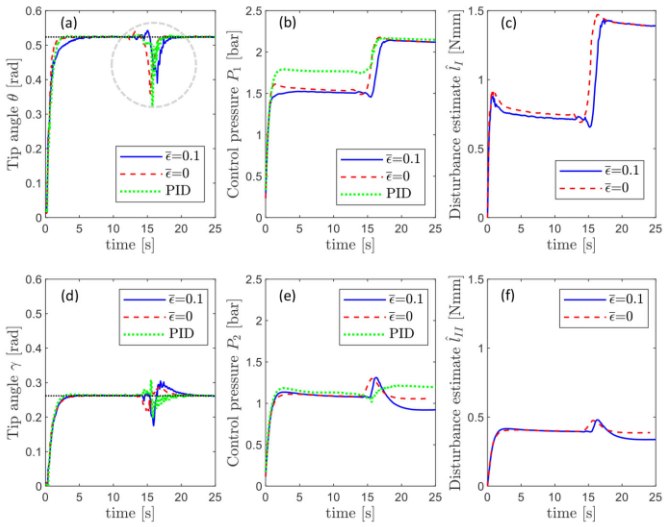

Figure 7. Experimental results with mass $m_0 = 1$ g attached at the tip of the manipulator at time $t = 12$ seconds (test setup shown Figure 1.e): time histories of the tip angle θ (a); and of the tip angle γ (d); control pressure P_1 (b); control pressure P_2 (e); disturbance estimate $\hat{l}_I$ (c); disturbance estimate $\hat{l}_{II}$ (f). The tuning parameters of controller (16) are $k_p = 0.5, k_{vI} = k_{vII} = 1, k_m = 20, \alpha = 10$, and $\bar{\varepsilon} = 0.1$ unless otherwise stated in the legend.

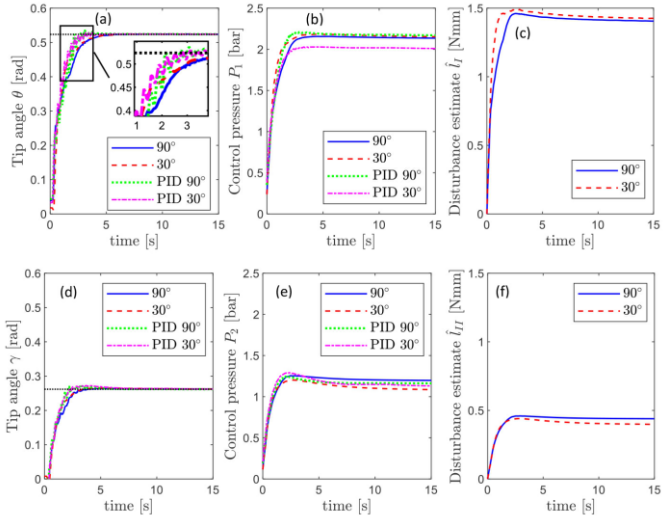

Figure 8. Experimental results with tip mass $m_0 = 1$ g for two orientations of the base frame (see legend): time histories of the tip angle θ (a); and tip angle γ (d); control pressure P_1 (b); control pressure P_2 (e); disturbance estimate $\hat{l}_I$ (c); disturbance estimate $\hat{l}_{II}$ (f). The tuning parameters of controller (16) are $k_p = 0.5, k_{vI} = k_{vII} = 1, k_m = 20, \alpha = 10$, and $\bar{\varepsilon} = 0.1$.

The experimental results without external forces using the controller (16) and different values of k_p are shown in Figure 6. The regulation goal has been correctly achieved but the disturbance estimates are not zero due to the presence of model uncertainties, which are treated as a lumped disturbance in (3). The disturbance estimates increase at larger rotations θ suggesting a potential discrepancy between the model (2) and the real system, due to the deformation of the partition walls between the internal chambers (see Figure 6.c). In this case, the system response of the PID is very similar to that of the controller (16) with $k_p = 0.5$ suggesting that the two might be equivalent in the same operating conditions. However, the control effort is visibly higher for the PID (see Figure 6.b).

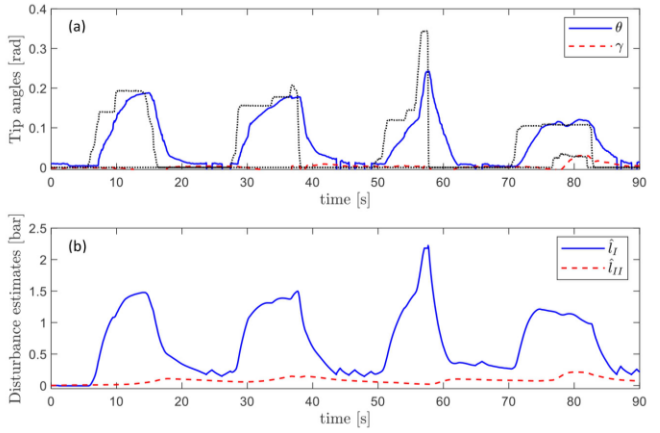

Figure 9. Experimental results for the setup shown Figure 1.f: time histories of the tip angles for a time-varying setpoint (a); disturbance estimates (b).

The time histories of the tip rotation in the presence of unknown time-varying external forces corresponding to two different loading conditions are shown in Figure 7 and Figure 8. In the first case, a mass $m_0 = 1$ gram (comparable to m_T) has been attached to the tip of the manipulator at time $t = 12$ seconds. This type of disturbance acts in the bending plane and also orthogonally to it, as shown by the angles θ and γ. Since u_0 injects additional damping in the closed-loop system (5), a larger value of $\bar{\varepsilon}$ reduces the maximum deviation from the prescribed equilibrium after the disturbance onset ($|\theta - \theta_d| = 0.13$ with $\bar{\varepsilon} = 0.1$; and $|\theta - \theta_d| = 0.16$ with $\bar{\varepsilon} = 0$) but also results in a slower transient (see Figure 7.a). In this case, the PID shows a larger deviation from the prescribed equilibrium ($|\theta - \theta_d| = 0.2$) and a higher control effort (see Figure 7.b). The disturbance estimates are computed with (15) and converge to a different value from the disturbance-free case because of m_0 (see Figure 7.c and 7.f).

In the second loading condition the tip mass m_0 has been attached at the start of the experiment and it produces bending moments that vary with the tip rotations θ and γ and with the orientation of the base frame. Two orientations of the manipulator have been considered: in the first case the bending plane is approximately aligned with gravity, while in the second it is inclined by approximately 30 degrees. Also in this case the controller (16) has correctly achieved the regulation goal in spite of the external disturbance (see Figure 8.a and 8.d) and the transient response is very similar for both orientations. Due to the adaptive law (15) which compensates the effect of the payload, the final values of the control pressures are slightly different (see Figure 8.b and 8.e). The adaptive estimate of the in-plane disturbance $\hat{l}_I$ and of the out-of-plane disturbance $\hat{l}_{II}$ converge to different values at different orientations of the bending plane with respect to gravity (see Figure 8.c and 8.f). In this case the transient response with the PID shows noticeable oscillations (see Figure 8.a) and the control input u_I is less consistent for different orientations. This occurs since the tip mass results in time-varying bending moments during the transient and suggests that the parameters of the PID might need to be re-tuned for different operating conditions. Although gain scheduling procedures could improve the performance of the

PID, they would require additional assumptions on the type and magnitude of the disturbances.

Additional plots showing the position errors $|\theta - \theta_d|$ and $|\gamma - \gamma_d|$, and the $L2$ norm of the control input corresponding to Figure 2, Figure 3, Figure 6, Figure 7, and Figure 8 are accessible at this link. Experimental results for the case of variable setpoint are shown in Figure 9 and in the Supplementary Video. The aim of the video is only to illustrate the performance of the manipulator with the controller (16) for a variable setpoint in the presence of time-varying disturbances and is not intended to demonstrate clinical use. In addition to the actuation and sensing hardware previously described, the setup includes an endoscopic camera (Shekar 5.5mm USB Camera) that shows the manipulator inside a cardiovascular phantom (see Figure 1.f), a second camera that provides an external view, and a joystick (Xbox 360 Controller) for the operator to define the setpoint (θ_d, γ_d). A scalpel blade is mounted at the tip of the manipulator to interact with a deformable obstacle (Bostik Blu tack). The results indicate that the regulation goal is achieved for a variable setpoint and in the presence of time-varying disturbances due to the contact with the deformable obstacle.

V. Conclusion and Future Work

A nonlinear adaptive controller has been proposed for a class of soft continuum manipulators with nonlinear uniform stiffness and nonlinear damping affected by time-varying disturbances. The control law compensates the effect of unknown external forces and of model uncertainties, and it is implementable with a single sensor that measures the tip orientation of the manipulator in a fixed base frame. Stability conditions for the prescribed equilibrium have been discussed highlighting their relationship with the tuning parameters and with physical damping. In particular, the stability analysis indicates that nonlinear damping is beneficial for stability, but that larger physical damping demands a less aggressive tuning of the controller parameters. This finding sheds new light on the role of damping in the control of underactuated mechanical system. The effectiveness of the controller has been assessed with simulations and with experiments on a soft continuum manipulator prototype that employs pneumatic actuation. The controller achieves the regulation goal producing a more consistent response across different operating conditions compared to a traditional PID scheme with equivalent tuning parameters. The simulation results suggest that the new control law improves the transient response compared to our prior implementations. The experimental results indicate that the control law reduces the deviation from the prescribed equilibrium and the unwanted vibrations that might be induced by external forces compared to the PID.

Nevertheless, the current study has a number of limitations. The proposed model assumes negligible twist thus it does not apply to manipulator designs for which twist is an actuated DOF or to disturbances that include twisting moments. The parameterization employed for the structural stiffness is not suitable for soft manipulators with variable section along the axis. In addition, the pressure dynamics might need to be modelled explicitly for larger manipulators supplied by different types of valves or through longer pipes. Moreover, actuator saturation could prevent the system from achieving the regulation goal in the presence of high disturbances. Finally, the controller relies on measurements of the tip orientation, which were achieved with an electromagnetic tracking system that has a limited range. In principle an inclinometer could represent an inexpensive alternative and could be more suitable for larger manipulators.

Future work shall aim to extend these results to soft continuum manipulators with variable section and to soft manipulators for which twist is an actuated DOF.

Appendix

The symmetric matrices $\mathcal{A}$ and $\mathcal{B}$ in (23) are defined as:

$$\mathcal{A} = \begin{bmatrix} k_{vII}/k_m^2 + R_0/(2k_m) & \star \\ k_{vII}/(2k_m^2) & R_0/(2nk_m) \end{bmatrix} \tag{A1}$$

$$\mathcal{B} = \begin{bmatrix} (R_0 - 2\alpha c_1 m_T L_T^2 - 2\mu)/(2k_m) & \star & \star \\ 0 & R_1/k_m & \star \\ -(1/k_m + \alpha^2 c_1 m_T L_T^2 + \mu\alpha)/2 & -(\alpha c_2 m_T L_T^2)/2 & \alpha \end{bmatrix}. \tag{A2}$$

Employing a Schur complement argument and recalling that $R_0 > 0, R_1 > 0$ (see *Assumption 3*) and that $\alpha > 0, k_m > 0, k_{vII} > 0$ by hypothesis, we have that $\mathcal{A} > 0$ if and only if:

$$(k_{vII}/2k_m^2)^2 - R_0\,(k_{vII}/k_m^2 + R_0/2k_m)/(2nk_m) < 0. \tag{A3}$$

The condition that follows from (A3) is

$$0 < k_{vII} < R_0 k_m\left(1 + \sqrt{n+1}\right)/n. \tag{A4}$$

References

[1] M. Cianchetti, C. Laschi, A. Menciassi, and P. Dario, "Biomedical applications of soft robotics," *Nat. Rev. Mater.*, vol. 3, no. 6, pp. 143–153, Jun. 2018.

[2] C. Wang, C. G. Frazelle, J. R. Wagner, and I. Walker, "Dynamic Control of Multi-Section Three-Dimensional Continuum Manipulators Based on Virtual Discrete-Jointed Robot Models," *IEEE/ASME Trans. Mechatronics*, pp. 1–11, Jun. 2020.

[3] S. Calo, J. H. Chandler, F. Campisano, K. L. Obstein, and P. Valdastri, "A Compression Valve for Sanitary Control of Fluid-Driven Actuators," *IEEE/ASME Trans. Mechatronics*, vol. 25, no. 2, pp. 1005–1015, Apr. 2020.

[4] F. Xu, H. Wang, J. Wang, K. W. S. Au, and W. Chen, "Underwater Dynamic Visual Servoing for a Soft Robot Arm with Online Distortion Correction," *IEEE/ASME Trans. Mechatronics*, vol. 24, no. 3, pp. 979–989, Jun. 2019.

[5] W. Liang, J. Cao, Q. Ren, and J. X. Xu, "Control of Dielectric Elastomer Soft Actuators Using Antagonistic Pairs," *IEEE/ASME Trans. Mechatronics*, vol. 24, no. 6, pp. 2862–2872, Dec. 2019.

[6] J. Burgner-Kahrs, D. C. Rucker, and H. Choset, "Continuum Robots for Medical Applications: A Survey," *IEEE Trans. Robot.*, vol. 31, no. 6, pp. 1261–1280, Dec. 2015.

[7] C. Tawk, H. Zhou, E. Sariyildiz, M. In Het Panhuis, G. Spinks, and G. Alici, "Design, Modeling and Control of a 3D Printed Monolithic Soft Robotic Finger with Embedded Pneumatic Sensing Chambers," *IEEE/ASME Trans. Mechatronics*, pp. 1–11, 2020.

[8] T. G. Thuruthel, Y. Ansari, E. Falotico, and C. Laschi, "Control Strategies for Soft Robotic Manipulators: A Survey," *Soft Robot.*, vol. 5, no. 2, pp. 149–163, Jan. 2018.

[9] M. Li, R. Kang, D. T. Branson, and J. S. Dai, "Model-Free Control for Continuum Robots Based on an Adaptive Kalman Filter," *IEEE/ASME Trans. Mechatronics*, vol. 23, no. 1, pp. 286–297, Feb. 2018.

[10] K.-H. Lee *et al.*, "Nonparametric Online Learning Control for Soft

Continuum Robot: An Enabling Technique for Effective Endoscopic Navigation," *Soft Robot.*, vol. 4, no. 4, pp. 324–337, Dec. 2017.
[11] V. Falkenhahn, T. Mahl, A. Hildebrandt, R. Neumann, and O. Sawodny, "Dynamic Modeling of Bellows-Actuated Continuum Robots Using the Euler–Lagrange Formalism," *IEEE Trans. Robot.*, vol. 31, no. 6, pp. 1483–1496, Dec. 2015.
[12] I. S. Godage, R. Wirz, I. D. Walker, and R. J. Webster, "Accurate and Efficient Dynamics for Variable-Length Continuum Arms: A Center of Gravity Approach," *Soft Robot.*, vol. 2, no. 3, pp. 96–106, Sep. 2015.
[13] F. Renda, F. Boyer, J. Dias, and L. Seneviratne, "Discrete Cosserat Approach for Multisection Soft Manipulator Dynamics," *IEEE Trans. Robot.*, vol. 34, no. 6, pp. 1518–1533, Dec. 2018.
[14] S. Grazioso, G. Di Gironimo, and B. Siciliano, "A Geometrically Exact Model for Soft Continuum Robots: The Finite Element Deformation Space Formulation," *Soft Robot.*, vol. 6, no. 6, pp. 1–22, Nov. 2018.
[15] J. Till, V. Aloi, and C. Rucker, "Real-time dynamics of soft and continuum robots based on Cosserat rod models," *Int. J. Rob. Res.*, vol. 38, no. 6, pp. 723–746, May 2019.
[16] O. Goury and C. Duriez, "Fast, Generic, and Reliable Control and Simulation of Soft Robots Using Model Order Reduction," *IEEE Trans. Robot.*, vol. 34, no. 6, pp. 1565–1576, Dec. 2018.
[17] T. Morales Bieze, A. Kruszewski, B. Carrez, and C. Duriez, "Design, implementation, and control of a deformable manipulator robot based on a compliant spine," *Int. J. Rob. Res.*, vol. 39, no. 14, pp. 1604–1619, Apr. 2020.
[18] V. Falkenhahn, A. Hildebrandt, R. Neumann, and O. Sawodny, "Dynamic Control of the Bionic Handling Assistant," *IEEE/ASME Trans. Mechatronics*, vol. 22, no. 1, pp. 6–17, Feb. 2017.
[19] C. M. Best, L. Rupert, and M. D. Killpack, "Comparing model-based control methods for simultaneous stiffness and position control of inflatable soft robots," *Int. J. Rob. Res.*, pp. 1–24, May 2020.
[20] P. Hyatt, D. Kraus, V. Sherrod, L. Rupert, N. Day, and M. Killpack, "Configuration Estimation for Accurate Position Control of Large-Scale Soft Robots," *IEEE/ASME Trans. Mechatronics*, vol. 24, no. 1, pp. 88–99, 2019.
[21] C. Della Santina *et al.*, "Controlling Soft Robots: Balancing Feedback and Feedforward Elements," *IEEE Robot. Autom. Mag.*, vol. 24, no. 3, pp. 75–83, Sep. 2017.
[22] C. Della Santina, R. K. Katzschmann, A. Bicchi, and D. Rus, "Model-based dynamic feedback control of a planar soft robot: trajectory tracking and interaction with the environment," *Int. J. Rob. Res.*, vol. 39, no. 4, pp. 490–513, Jan. 2020.
[23] C. Della Santina and D. Rus, "Control oriented modeling of soft robots: The polynomial curvature case," *IEEE Robot. Autom. Lett.*, vol. 5, no. 2, pp. 290–298, Apr. 2020.
[24] I. A. Gravagne, C. D. Rahn, and I. D. Walker, "Large deflection dynamics and control for planar continuum robots," *IEEE/ASME Trans. Mechatronics*, vol. 8, no. 2, pp. 299–307, Jun. 2003.
[25] J. Zou and G. Gu, "High-precision tracking control of a soft dielectric elastomer actuator with inverse viscoelastic hysteresis compensation," *IEEE/ASME Trans. Mechatronics*, vol. 24, no. 1, pp. 36–44, Feb. 2019.
[26] H. Pan, X. Jing, W. Sun, and H. Gao, "A Bioinspired Dynamics-Based Adaptive Tracking Control for Nonlinear Suspension Systems," *IEEE Trans. Control Syst. Technol.*, vol. 26, no. 3, pp. 903–914, May 2018.
[27] R. Ortega, M. W. Spong, F. Gomez-Estern, and G. Blankenstein, "Stabilization of a class of underactuated mechanical systems via interconnection and damping assignment," *IEEE Trans. Automat. Contr.*, vol. 47, no. 8, pp. 1218–1233, Aug. 2002.
[28] D. Ross, M. P. Nemitz, and A. A. Stokes, "Controlling and Simulating Soft Robotic Systems: Insights from a Thermodynamic Perspective," *Soft Robot.*, vol. 3, no. 4, pp. 170–176, Dec. 2016.
[29] E. Franco and A. Garriga-Casanovas, "Energy Shaping Control of Soft Continuum Manipulators with in-plane Disturbances," *Int. J. Rob. Res.*, pp. 1–20, Mar. 2020.
[30] E. Franco, A. Garriga Casanovas, F. Rodriguez y Baena, and A. Astolfi, "Model based adaptive control for a soft robotic manipulator," in *2019 IEEE Conference on Decision and Control*, 2019, pp. 1019–1024.
[31] A. Astolfi, D. Karagiannis, and R. Ortega, *Nonlinear and Adaptive Control with Applications*. Berlin, 2007.
[32] A. Astolfi and R. Ortega, "Immersion and invariance: A new tool for stabilization and adaptive control of nonlinear systems," *IEEE Trans. Automat. Contr.*, vol. 48, no. 4, pp. 590–606, 2003.
[33] K. Chen and A. Astolfi, "I&I Adaptive Control for Systems with Varying Parameters," in *2018 IEEE Conference on Decision and Control*, 2018, pp. 2205–2210.
[34] F. Gómez-Estern and A. J. Van der Schaft, "Physical Damping in IDA-PBC Controlled Underactuated Mechanical Systems," *Eur. J. Control*, vol. 10, no. 5, pp. 451–468, Jan. 2004.
[35] A. Garriga-Casanovas, I. Collison, and F. Rodriguez y Baena, "Toward a Common Framework for the Design of Soft Robotic Manipulators with Fluidic Actuation," *Soft Robot.*, vol. 5, no. 5, pp. 622–649, Aug. 2018.
[36] K. Suzumori, "Elastic materials producing compliant robots," *Rob. Auton. Syst.*, vol. 18, no. 1–2, pp. 135–140, Jul. 1996.
[37] L. L. Howell, A. Midha, and T. W. Norton, "Evaluation of Equivalent Spring Stiffness for Use in a Pseudo-Rigid-Body Model of Large-Deflection Compliant Mechanisms," *J. Mech. Des.*, vol. 118, no. 1, p. 126, Mar. 1996.
[38] S. J. Elliott, M. G. Tehrani, and R. S. Langley, "Nonlinear damping and quasi-linear modelling," *Philos. Trans. R. Soc. A Math. Phys. Eng. Sci.*, vol. 373, no. 2051, pp. 1–30, Sep. 2015.
[39] E. Franco, F. Rodriguez Y Baena, and A. Astolfi, "Robust Dynamic State Feedback for Underactuated Systems with Linearly Parameterized Disturbances," *Int. J. Robust Nonlinear Control*, vol. 30, no. 10, pp. 4112–4128, 2020.

Enrico Franco received the MSc degree in Mechanical Engineering from Politecnico di Torino, Italy, and a Ph.D. degree in medical robotics from Imperial College London. He is currently a Research Associate in the MiM Lab, Mechanical Engineering Department. His research interests include medical robotics, nonlinear control, and its applications to soft robotics.

Arnau Garriga-Casanovas received the BSc and the MSc degree in Aeronautical Engineering from Polytechnic University of Catalonia, Spain, and the Eng.D. degree from Imperial College London. He is currently a Research Associate in the NDE group, Mechanical Engineering Department. His research interests include soft robotics, nonlinear dynamics, and non-destructive evaluation.

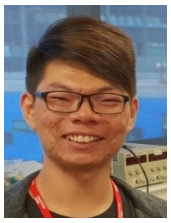

Jacky Tang received the BEng degree in Mechanical Engineering from Universiti Teknology Malaysia, and the MSc degree in Control Systems from Imperial College London. He is currently working as mechanical design engineer at Welford Manufacturing Sdn Bhd, Malaysia. His research interests include nonlinear control theory, medical robotics, and soft robotics.

Ferdinando Rodriguez y Baena holds a First Class Honors degree in Mechatronics and Manufacturing Systems Engineering from King's College London and a Ph.D. degree in medical robotics from Imperial College. He is a Professor of Medical Robotics with the Department of Mechanical Engineering, Imperial College. He is the director of the MiM Lab and of the Medical Engineering group, and the Engineering Co-Director of the Hamlyn Centre. His research interest includes the application of mechatronic systems to clinical training, diagnostics, and surgical intervention.

Alessandro Astolfi (F'09) received the M.S. degree in electrical engineering from the University of Rome, the M.Sc. degree in information engineering and the Ph.D. degree (with medal of honor) in discontinuous stabilization of nonholonomic systems from ETH-Zurich, Switzerland, and the Ph.D. degree in nonlinear robust control from the University of Rome "La Sapienza," Italy. He is Professor of Non-linear Control Theory in the Electrical and Electronic Engineering Department, Imperial College, London (UK), and Professor with the Dipartimento di Informatica, Sistemi e Produzione, University of Rome Tor Vergata. His research interests are focused on mathematical control theory and control applications, discontinuous stabilization, and adaptive control.